

Vortex instability in molybdenum-germanium superconducting films

Manlai Liang and Milind N. Kunchur*

Department of Physics and Astronomy, University of South Carolina, Columbia, South Carolina 29208, USA

(Received 21 August 2010; published 18 October 2010)

We studied the high driving force regime of the current-voltage transport response in the mixed state of amorphous molybdenum-germanium superconducting films to the point where the flux flow becomes unstable. The observed nonlinear response conforms with the classic Larkin-Ovchinnikov picture with a quasiparticle-energy-relaxation rate dominated by the quasiparticle recombination process. The measured energy relaxation rate was found to have a magnitude and temperature dependence in agreement with theory.

DOI: [10.1103/PhysRevB.82.144517](https://doi.org/10.1103/PhysRevB.82.144517)

PACS number(s): 74.40.Gh, 74.25.Uv, 72.15.Lh, 73.50.Gr

I. INTRODUCTION AND THEORY

In a type-II superconductor, magnetizing fields between the lower critical field H_{c1} and upper critical field H_{c2} introduce flux vortices containing a quantum of flux $\Phi_0 = h/2e$. A transport electric current density j perpendicular to the vortices and to exerts a ‘‘Lorentz’’ driving force $F_L = j\Phi_0$. The consequent vortex motion generates an electric field $E = vB$ and is opposed by a viscous drag ηv (where η is the coefficient of viscosity and v the vortex velocity) so that in steady state $j\Phi_0 = \eta v \propto E$ and the response is Ohmic as long as the flow is not hindered by pinning. This regime of flux motion corresponds to free flux flow (FFF). While superficially the physics appears simple, and bears resemblance to a hydrodynamic system, this resemblance and apparent simplicity are deceiving. First of all the so-called Lorentz force in a superconductor actually has the opposite direction to the usual electromagnetic Lorentz force and while it has the right magnitude $F_L = j\Phi_0$, the derivation of this expression is not completely trivial.^{1–6} Second the hydrodynamic analogy leads to the expectation that a narrower vortex would have a lower drag coefficient. Under normal circumstances the reality is just the opposite: dissipation in and around the core of a vortex arises from generated electric fields acting upon normal quasiparticles leading to Ohmic dissipation⁷ and from irreversible entropy transfer occurring between the leading and trailing edges of moving vortices.⁸ These dissipative processes increase with the order-parameter gradient so that η is roughly inversely proportional to the vortex core area. Thus under normal circumstances η drops as the the vortex expands and hence the flux-flow resistance goes up with temperature.^{9,10}

The Ohmic FFF regime discussed above ceases as j and E are increased to high values that alter the superconducting state. If the electron-electron scattering time τ_{ee} is short compared to the electron-phonon scattering time τ_{ep} , the distribution function of the quasiparticles becomes thermalized and a finite power dissipation density jE simply raises the electron temperature to a value T' above the phonon and substrate temperatures, T_p and T_0 , respectively. This causes an expansion of the vortex core and a drop in viscosity leading to a nonmonotonic (‘‘N’’ shaped) $j(E)$ curve and a consequent instability. Such a hot-electron instability model was developed and experimentally verified by us in our earlier work.^{9,11}

A more intricate scenario, proposed by Larkin and Ovchinnikov^{12,13} (LO), arises when $\tau_{ee} > \tau_{ep}$. In this case the quasiparticle distribution function acquires a nonthermal shape and the vortex dynamics are altered in a complicated and less obvious way. At high E the quasiparticle population in the core reduces while it increases outside the core, thus causing the vortex to shrink while simultaneously reducing the contrast in quasiparticle density between the two regions. Thus the gradient in the order parameter Δ is not boosted to the extent anticipated by the reduced vortex size. In the meanwhile, the diminished quasiparticle population in the core tends to lessen the dissipation and reduce the drag. Thus overall η declines despite the shrinking in size with increasing E . Like the hot-electron case discussed earlier, this again leads to a nonmonotonic $j(E)$ curve and a vortex instability. The LO instability has been observed in previous experiments^{14–24} and the combination of heating effects and the LO mechanism have been considered by various authors.^{25–29}

The relative magnitudes of τ_{ee} and τ_{ep} govern which mechanism dominates the instability. Standard estimates³⁰ for the scattering times $\tau_{ee} = r\hbar\epsilon_F/k_B^2T^2$ and $\tau_{ep} = r^3\hbar T_D^2/k_B T^3$ (where T_D is the Debye temperature and $r < 1$ is the phonon reflection coefficient at the film-substrate interface arising from acoustic mismatch) give a crossover temperature of $T_X = r^2 k_B T_D^2 / \epsilon_F$. In the present work, we investigated amorphous molybdenum-germanium (MoGe) films, which have (estimating from known parameters^{31,32}) $T_D = 260$ K and $\epsilon_F \approx 10$ eV, and thus have $T_X < 0.6r^2$ K. Since $r < 1$, T_X will be well below the temperature range of our experiment (3–6 K). Thus we expect the nonlinear $j(E)$ response to be dictated by the LO mechanism, which is indeed born out by our data.

In the LO theory, the nonlinear flux-flow conductivity at high E is given by (Eqs. 38 and 53 of Ref. 12)

$$\sigma(E) \approx \sigma_f \left\{ \frac{1}{1 + \left(\frac{E}{E^*}\right)^2 + c\sqrt{1-t}} \right\} \approx \frac{\sigma_f}{1 + \left(\frac{E}{E^*}\right)^2} \quad (1)$$

in terms of the free-flux-flow value σ_f of the linear regime ($E \rightarrow 0$ limit in the absence of pinning) and E^* the critical electric field at which j attains its maximum value before the $j(E)$ curve enters a region of negative differential conductivity. $t = T/T_c$ is the reduced temperature (T_c is the supercon-

ducting transition temperature), c is an unknown constant of order unity and E^* is given by

$$E^{*2} = \frac{D\sqrt{14\zeta(3)(1-t)}}{\pi\tau_\varepsilon} B^2, \quad (2)$$

where D is the diffusion constant, $\zeta(x)$ is the Riemann zeta function, and τ_ε is the energy relaxation time.

In our previous work³³ we found that the expressions for $\sigma_f(0)$ in Ref. 13 (their Eqs. 22 and 30) did not fit the data well over a significant range. Instead the following expression:³³

$$\sigma_f \approx \sigma_n + \sigma_n \left(\frac{1-b}{vb} \right) \quad (3)$$

based on the mean-field result of time-dependent Ginzburg-Landau (TDGL) theory,^{34–39} more accurately represented the behavior over an extended range; here $b=B/\mu_0 H_{c2}$ is the reduced magnetic field (H_{c2} is the upper critical magnetizing field) and $\nu \sim 0.3$ is a dimensionless constant. The right-hand side of Eq. (3) represents a two-fluid-model sum of the normal conductivity σ_n and the flux-flow conductivity contribution. The first term is negligible compared to the second term for the range of conditions where we study the LO nonlinear effect (i.e., our mixed-state conductivity is far higher than the normal conductivity) and also the σ_n term remains constant and is not affected by E and B fields. Thus combining Eq. (1) with the second term of Eq. (3) gives the following nonlinear $j(E)$ relationship:

$$j = E \left[\left\{ \sigma_n \left(\frac{1-b}{vb} \right) \right\} \left\{ \frac{1}{1 + (E/E^*)^2} \right\} \right]. \quad (4)$$

Note that this nonlinear function is only valid until the vortex stops shrinking, which occurs at a field¹³ $E_s \sim E^*/(1-t)^{1/4}$. At very high E the system eventually enters the normal state and then $\sigma = \sigma_n$.

II. EXPERIMENTAL TECHNIQUES

The samples A, B, and C used in this experiment are exactly the same as the samples A, B, and C used in our prior work on free flux flow.³³ The samples consist of MoGe films of thickness 50 nm sputtered onto silicon substrates with 200-nm-thick oxide layers using an alloy target of atomic composition $\text{Mo}_{0.79}\text{Ge}_{0.21}$. The deposition system had a base pressure of 2×10^{-7} Torr and the argon-gas working pressure was maintained at 3 mTorr during the sputtering. The growth rate was 0.15 nm/s. The samples were patterned into bridges of length $l=102 \mu\text{m}$ and width $w=6 \mu\text{m}$ using photolithography and argon ion milling. Some parameters of the samples are as follows: Sample A: $T_c=5.56$ K, $R_n=555 \Omega$, $\mu_0 H'_{c2}=-3.13$ T/K, and $D=0.35 \text{ cm}^2/\text{s}$. Sample B: $T_c=5.41$ K, $R_n=555 \Omega$, $\mu_0 H'_{c2}=-3.13$ T/K, and $D=0.35 \text{ cm}^2/\text{s}$. Sample C: $T_c=5.01$ K, $R_n=630 \Omega$, $\mu_0 H'_{c2}=-3.0$ T/K, and $D=0.37 \text{ cm}^2/\text{s}$. Here, R_n is the normal-state resistance, $H'_{c2}=dH_{c2}/dT|_{T_c}$ is the upper-critical-field slope, and the diffusion coefficient D was calculated from⁴⁰ $D=-8k_B/2\pi e\mu_0 H'_{c2}$.

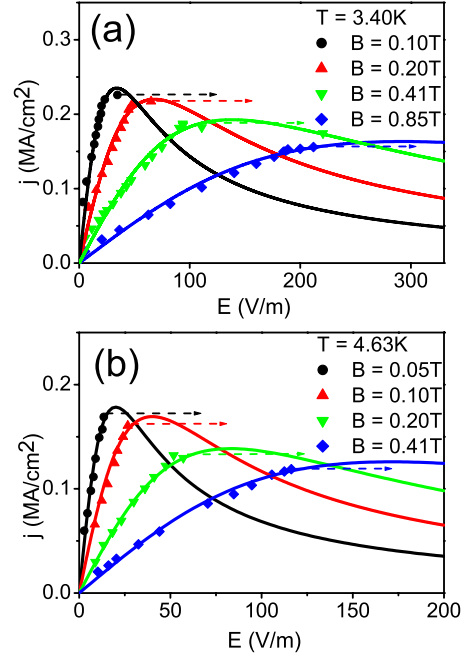


FIG. 1. (Color online) j versus E curves for sample B at two temperatures (a) 3.40 and (b) 4.63 K, at indicated B values. The symbols correspond to the measured data and the solid lines correspond to Eq. (4). The dashed arrows indicate the observed jump in E . For the theoretical curves, ν and E^* were adjusted to the following values: For $T=3.40$ K, $\nu \approx 0.3$, and $E^*=34, 68, 138,$ and 292 V/m in the order of ascending B . For $T=4.63$ K, $\nu \approx 0.2$, and $E^*=20, 40, 83,$ and 171 V/m.

The cryostat was a Cryomech PT405 pulsed-tube closed-cycle refrigerator that went down to about 3.2 K. It was fitted inside a 1.3 T GMW 3475–50 water-cooled copper electromagnet. Calibrated cernox and hall sensors monitored T and B respectively. The electrical transport measurements were made with an in-house built pulsed current source, preamplifier circuitry, and a LeCroy model 9314A digital storage oscilloscope. The pulse durations are 20 μs or less, with duty cycles in the few ppm range to reduce macroscopic heating of the film. Our previous review papers^{41,42} give further details about the measurement technique and the thermal analysis.

III. DATA AND ANALYSIS

Figure 1 shows some examples of nonlinear $j(E)$ curves. j (and hence the viscous drag force) has a local maximum value of j^* at the instability field E^* . In a current biased circuit, where the source resistance is larger than the sample resistance as is the case here, E jumps (indicated by arrows) upon increasing j to the vicinity of the intrinsic j^* . In a voltage biased measurement, where the source resistance is lower than the sample's, there will not be a jump in E and instead j will be seen to decrease. The macroscopically averaged behavior will have a negative dj/dE and the flux matter fragments into compressional,⁴³ shear⁴⁴ or other types of elastic domains such that any given domain is moving in a response region with $dj/dE > 0$ locally. The macroscopic

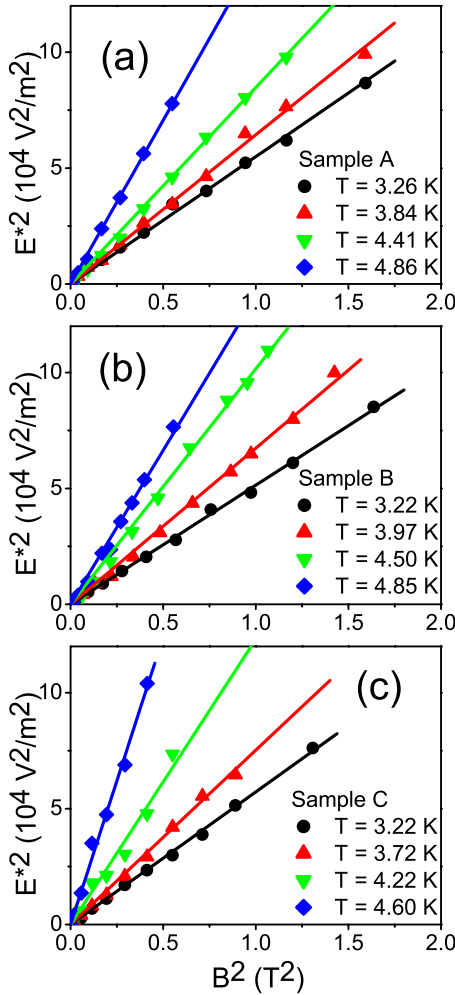


FIG. 2. (Color online) E^{*2} versus B^2 for samples A, B, and C at indicated temperatures showing proportionality between the two quantities as per Eq. (2). The lines are least-squares linear fits to the data (symbols).

$j(E)$ curve will then not follow the primitive curve [e.g., Eq. (4)] but will show steps in the region where $dj/dE < 0$. In the present experiment we are only concerned with the region of the transport response up to E^* where $dj/dE > 0$ macroscopically.

The solid lines in Fig. 1 are fits to Eq. (4) and are seen to follow the trends of the data. The parameters ν and E^* (location of peak) were adjusted to improve the fits, but have fit values of the expected magnitudes: $\nu \sim 0.3$ and E^* from the peaks is slightly higher than the position of the actual jumps, which is to be expected and has been observed by others (e.g., Ref. 21). For subsequent analysis, we take E^* to be the actual measured value of E at the threshold of the jump.

Figure 2 plots E^{*2} , obtained from the $j(E)$ curves as discussed above, against B^2 . In agreement with Eq. (2), the two quantities are directly proportional to each other (i.e., the critical vortex velocity $v^* = E^*/B$ is independent of B). From the measured slope and Eq. (2), we obtain the energy relaxation time τ_e . Figure 3 plots the corresponding relaxation rate τ_e^{-1} against the reduced temperature for each of the three samples.

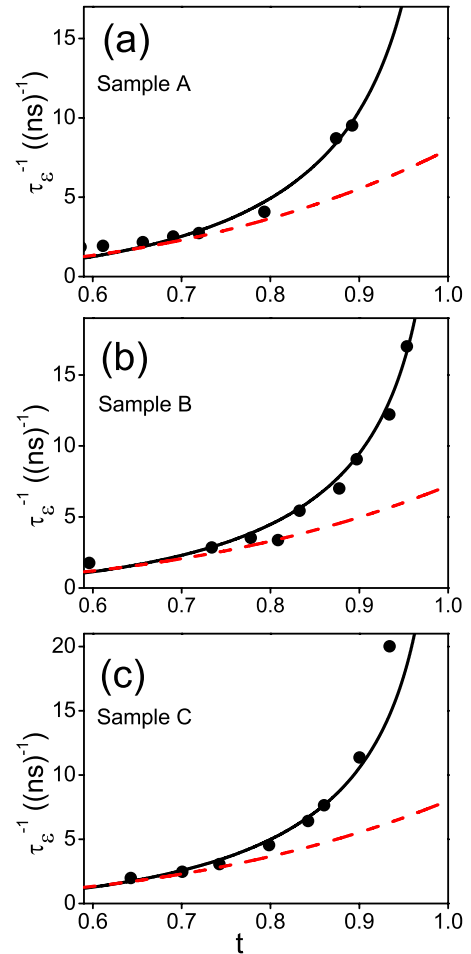


FIG. 3. (Color online) Temperature dependence of the energy-relaxation rate. The symbols represent the experimental values deduced from Eq. (2) and the measured E^* . The solid black lines are fits to Eq. (5) (quasiparticle recombination process) with the values $\mathcal{T} = 3.4 \times 10^{-11}$ s, 3.7×10^{-11} s, and 3.3×10^{-11} s for samples A–C, respectively. The dashed red lines are fits to $\tau_e^{-1} = at^{7/2}$ [expected for inelastic quasiparticle-phonon scattering (Ref. 45)] with $a = 8 \times 10^9$ s $^{-1}$, 7×10^9 s $^{-1}$, and 8×10^9 s $^{-1}$ for samples A–C respectively.

As discussed in the introduction, the LO effect occurs when τ_{ee} is long compared with τ_{ep} , resulting in a nonthermal shape of the quasiparticle distribution function. The extent of the distribution function distortion is controlled by the rate of energy relaxation from quasiparticles to phonons, which occurs through two processes: one process is the inelastic scattering between a quasiparticle and a phonon and the other is the recombination of two quasiparticles to form a Cooper pair with the emission of a phonon. As discussed by Kaplan *et al.*,⁴⁵ the energy relaxation is mainly dominated by the latter recombination process which has a rate that can be written as

$$\tau_e^{-1} = \mathcal{T}^{-1} \left(\frac{k_B T}{\Delta} \right)^{1/2} \exp\left(-\frac{\Delta}{k_B T}\right), \quad (5)$$

where \mathcal{T} is a temperature-independent characteristic time constant (in the terminology of Kaplan *et al.*,⁴⁵ $\mathcal{T} \approx \tau_0/55$) and Δ is the temperature-dependent superconducting energy gap. Taking the Bardeen-Cooper-Schrieffer (BCS) temperature dependence for Δ we are able to fit the data in Fig. 3 with Eq. (5) (solid lines) with $\mathcal{T} \approx 3.5 \times 10^{-11}$ s. As can be seen, the measured functional form of $\tau_e^{-1}(t)$ is in agreement with Eq. (5). While there is insufficient information in the literature to theoretically compute the magnitude of \mathcal{T} for comparison, Table I of Ref. 45 lists values of τ_0 ($\approx 55 \times \mathcal{T}$) for various other materials. Although there is an enormous range in \mathcal{T} —from 8×10^{-13} to 4×10^{-5} s for various materials—it is interesting to observe that tantalum with about the same T_c (4.5 K) and T_D (240 K) as MoGe (for which $T_c \approx 5.3$ K and $T_D \approx 260$ K) has a value of \mathcal{T} (3.3×10^{-11} s) that is comparable to the one we obtained for MoGe (3.5×10^{-11} s). (T_c and T_D are parameters that are indicative of the electron-phonon coupling and phonon density of states, respectively.) If quasiparticle-phonon scattering is the dominant relaxation process, rather than quasiparticle recombination, then the rate is given by a function of the form⁴⁵ $\tau_e^{-1} \propto t^{7/2}$ instead of Eq. (5). This power-law function (taken with an adjustable constant of proportionality a) is plotted as dashed red lines on Fig. 3 and is clearly at odds with the data. Thus our study of the vortex instability is able to distinguish the two routes of energy decay and provides a confirmation of the recombination rate expression of Eq. (5).

IV. CONCLUSIONS

In conclusion, we have studied the high driving force regime of vortex dynamics in one of the simplest and nearly model superconductors (unpinned, isotropic, low-temperature, weak-coupling BCS, etc.). In recent work³³ we found that for the FFF regime these MoGe films provided a detailed confirmation of the TDGL mean-field prediction for $\sigma_f(0)$, while the LO expressions for the same regime showed very limited applicability. On the other hand in the present work we find that the LO expression [Eq. (1)] for the non-linear modulation factor for $\sigma_f(0)$ and the LO result [Eq. (2)] for the relationship between the instability electric field E^* and the energy relaxation time τ_e , are well obeyed in this system. Furthermore we were able to distinguish between the two principal quasiparticle-phonon energy relaxation processes and confirm the predicted temperature dependence [Eq. (5)] for the recombination process. Both regimes of instability, the hot electron as well as the distribution-function type, thus provide a valuable tool for investigating key scattering processes through the response of the mixed state.

ACKNOWLEDGMENTS

The authors gratefully acknowledge Jiong Hua, Zhili Xiao, James M. Knight, and Boris I. Ivlev. This work was supported by the U. S. Department of Energy under Grant No. DE-FG02-99ER45763.

*Corresponding author; kunchur@sc.edu;
http://www.physics.sc.edu/kunchur

- ¹M. Tinkham, *Introduction to Superconductivity* (McGraw-Hill, New York, 1996).
- ²P. G. de Gennes, *Superconductivity of Metals and Alloys* (Benjamin, New York, 1966).
- ³O. Narayan, *J. Phys. A* **36**, L373 (2003).
- ⁴D.-X. Chen, J. J. Moreno, A. Hernando, A. Sanchez, and B.-Z. Li, *Phys. Rev. B* **57**, 5059 (1998).
- ⁵J. I. Castro and A. Lopez, *J. Low Temp. Phys.* **135**, 15 (2004).
- ⁶P. Ao and D. J. Thouless, *Phys. Rev. Lett.* **70**, 2158 (1993).
- ⁷J. Bardeen and M. J. Stephen, *Phys. Rev.* **140**, A1197 (1965).
- ⁸M. Tinkham, *Phys. Rev. Lett.* **13**, 804 (1964).
- ⁹M. N. Kunchur, *Phys. Rev. Lett.* **89**, 137005 (2002).
- ¹⁰D. Y. Vodolazov and F. M. Peeters, *Phys. Rev. B* **76**, 014521 (2007).
- ¹¹J. M. Knight and M. N. Kunchur, *Phys. Rev. B* **74**, 064512 (2006).
- ¹²A. I. Larkin and Yu. N. Ovchinnikov, *Zh. Eksp. Teor. Fiz.* **68**, 1915 (1975) [*Sov. Phys. JETP* **41**, 960 (1976)].
- ¹³A. I. Larkin and Yu. N. Ovchinnikov, in *Nonequilibrium Superconductivity*, edited by D. N. Langenberg and A. I. Larkin (Elsevier, Amsterdam, 1986), Chap. 11.
- ¹⁴L. E. Musienko, I. M. Dmitrenko, and V. G. Volotskaya, *Pis'ma Zh. Eksp. Teor. Fiz.* **31**, 603 (1980) [*JETP Lett.* **31**, 567 (1980)].
- ¹⁵W. Klein, R. P. Huebener, S. Gauss, and J. Parisi, *J. Low Temp. Phys.* **61**, 413 (1985).

- ¹⁶S. G. Doettinger, R. P. Huebener, R. Gerdemann, A. Kühle, S. Anders, T. G. Träuble, and J. C. Villégier, *Phys. Rev. Lett.* **73**, 1691 (1994).
- ¹⁷A. V. Samoilov, M. Konczykowski, N.-C. Yeh, S. Berry, and C. C. Tsuei, *Phys. Rev. Lett.* **75**, 4118 (1995).
- ¹⁸Z. L. Xiao and P. Ziemann, *Phys. Rev. B* **53**, 15265 (1996).
- ¹⁹S. G. Doettinger, S. Kittelberger, R. P. Huebener, and C. C. Tsuei, *Phys. Rev. B* **56**, 14157 (1997).
- ²⁰B. J. Ruck, H. J. Trodahl, J. C. Abele, and M. J. Geselbracht, *Phys. Rev. B* **62**, 12468 (2000).
- ²¹D. Babić, J. Bentner, C. Sürgers, and C. Strunk, *Phys. Rev. B* **69**, 092510 (2004).
- ²²A. A. A. Armenio, C. Bell, J. Aarts, and C. Attanasio, *Phys. Rev. B* **76**, 054502 (2007).
- ²³G. Grimaldi, A. Leo, A. Nigro, S. Pace, and R. P. Huebener, *Phys. Rev. B* **80**, 144521 (2009).
- ²⁴G. Grimaldi, A. Leo, D. Zola, A. Nigro, S. Pace, F. Laviano, and E. Mezzetti, *Phys. Rev. B* **82**, 024512 (2010).
- ²⁵A. I. Bezuglyj and V. A. Shklovskij, *Physica C* **202**, 234 (1992).
- ²⁶A. Gurevich and G. Ciovati, *Phys. Rev. B* **77**, 104501 (2008).
- ²⁷Z. L. Xiao, P. Voss-de Haan, G. Jakob, and H. Adrian, *Phys. Rev. B* **57**, R736 (1998).
- ²⁸Z. L. Xiao, P. Voss-de Haan, G. Jakob, Th. Kluge, P. Haibach, H. Adrian, and E. Y. Andrei, *Phys. Rev. B* **59**, 1481 (1999).
- ²⁹C. Peroz and C. Villard, *Phys. Rev. B* **72**, 014515 (2005).
- ³⁰A. Abrikosov, *Fundamentals of the Theory of Metals* (North-Holland, Amsterdam, 1988).

- ³¹W. L. Carter, Ph.D. thesis, Stanford University, 1983.
- ³²J. M. Graybeal, Ph.D. thesis, Stanford University, 1985.
- ³³M. Liang, M. N. Kunchur, J. Hua, and Z. Xiao, *Phys. Rev. B* **82**, 064502 (2010).
- ³⁴A. Schmid, *Phys. Kondens. Mater.* **5**, 302 (1966).
- ³⁵C. Caroli and K. Maki, *Phys. Rev.* **164**, 591 (1967).
- ³⁶G. Vecris and R. A. Pelcovits, *Phys. Rev. B* **44**, 2767 (1991).
- ³⁷S. Ullah and A. T. Dorsey, *Phys. Rev. B* **44**, 262 (1991).
- ³⁸A. T. Dorsey, *Phys. Rev. B* **46**, 8376 (1992).
- ³⁹R. J. Troy and A. T. Dorsey, *Phys. Rev. B* **47**, 2715 (1993).
- ⁴⁰L. P. Gorkov, *Zh. Eksp. Teor. Fiz.* **36**, 1918 (1959) [*Sov. Phys. JETP* **9**, 1364 (1959)]; L. P. Gorkov, *Zh. Eksp. Teor. Fiz.* **37**, 1407 (1959) [*Sov. Phys. JETP* **10**, 998 (1960)].
- ⁴¹M. N. Kunchur, *Mod. Phys. Lett. B* **9**, 399 (1995).
- ⁴²M. N. Kunchur, *J. Phys.: Condens. Matter* **16**, R1183 (2004).
- ⁴³M. N. Kunchur, B. I. Ivlev, and J. M. Knight, *Phys. Rev. Lett.* **87**, 177001 (2001).
- ⁴⁴M. N. Kunchur, B. I. Ivlev, and J. M. Knight, *Phys. Rev. B* **66**, 060505 (2002).
- ⁴⁵S. B. Kaplan, C. C. Chi, D. N. Langenberg, J. J. Chang, S. Jafarey, and D. J. Scalapino, *Phys. Rev. B* **14**, 4854 (1976).